Application of the temperature-sensitive paint method for quantitative measurements in water*

Jonathan Lemarechal[¶,†], C. Klein[¶], D. Puckert[◦], U. Rist[◦]

[¶] Institute of Aerodynamics and Flow Technology, German Aerospace Center (DLR),
Bunsenstraße 10, D-37073 Göttingen, Germany

[◦] Institute for Aerodynamics and Gas Dynamics, University of Stuttgart,
Pfaffenwaldring 21, D-70569 Stuttgart, Germany

Abstract

In this paper the characteristics of a Europium-based temperature-sensitive paint (TSP) in polyurethane (PUR) clear coat submerged in water are investigated. It is shown that the temperature sensitivity is not affected by water. However, the optical transmission of the PUR is reduced, which reduces the measurable emission of the TSP. Furthermore, a TSP measurement in the laminar water channel at the Institute of Aerodynamics and Gas Dynamics, University of Stuttgart, was set up. In this experiment the skin friction field for two types of roughness elements, i.e., a truncated cylinder and an array of cuboids, in a Blasius-like boundary layer is investigated. Additionally, the temperature field was recorded with sub-millimeter resolution while an artificial heat flux was applied. A modification of the Colburn analogy is used to derive the skin friction from the temperature measurement. Skin friction results derived from velocity measurements are in good agreement with the TSP results. The experimental setup provides a resolution of the temperature and skin friction measurement of $(\Delta T)_{min} < 0.007\,\mathrm{K}$ *and* $(\Delta\tau)_{min} \leq 4.01 \times 10^{-5}\,\mathrm{N/m^2}$ *(*$\leq$*1 % skin friction of the undisturbed flow), respectively. Additionally the uncertainty of the temperature and skin friction measurement is analyzed.*

Keywords — *Temperature-Sensitive Paint, TSP, skin friction measurement, roughness elements, laminar water channel*

1. Introduction

textwidth: 17.19754cm linewidth: 8.29881cm

The surface-temperature distribution is an important quantity to be measured in experimental aerodynamics, e.g., heat exchangers and re-entry vehicles, and in fundamental research, e.g., Rayleigh-Bénard convection (Ahlers et al., 2019). From the temperature measurements the heat flux (Le Sant et al., 2002; Nakakita et al., 2003) or skin friction (Reynolds, 1874; Lin, 1994) can be derived. Experimental skin friction measurements are important for the development of streamlined vehicles such as aircraft or ships and their assessment. Furthermore, skin friction measurements are necessary in fundamental aerodynamic research (Rudolph, 2011) and in the development of drag reduction methods like the upstream flow deformation method (Wassermann and Kloker, 2002), spanwise velocity gradient method (Fransson et al., 2005), and riblets (Walsh, 1990).

Several optical measurement techniques are applied in wind tunnel or water facility experiments to measure surface temperatures: thermochromic liquid crystals (Gaudet and Gell, 1989), infrared thermography (Thomann and Frisk, 1968), and temperature-sensitive paint (Liu and Sullivan, 2005). All methods are spatial and non-intrusive. Besides temperature measurements these techniques are widely used for qualitative skin friction measurements, i.e., surface based flow visualizations, in a large variety of test facilities (Klein, 1968; Haselbach et al., 1995; Zhong et al., 1999; Peake et al., 1977; Bouchardy et al., 1983; Quast, 1987; Fey and Egami, 2007; Iijima et al., 2003). In addition to the qualitative skin friction visualization, the transition location (Fey and Egami, 2007) and the relative skin friction vector field can be derived. The latter can be calculated as an inverse problem by optical flow algorithms (Liu and Woodiga, 2011) and saddle points, convergence and convection lines can be determined (Miozzi et al., 2016, 2019b).

A quantitative evaluation of the skin friction magnitude from a temperature field on a flat plate with laminar flow and a laminar flow disturbed by a trip wire was performed by Rudolph (2011) from measurements with an infrared camera. Furthermore, Miozzi et al. (2019a) derived the skin friction based on the Taylor hypothesis, i.e. crosscorrelation of temperature fluctuations. The displacement of a tempera-

*Citation and credit: Lemarechal, J., Klein, C., Puckert, D.P., Rist, U.: Application of the temperature-sensitive paint method for quantitative measurements in water. Meas. Sci. Technol. (2021) 32:10 doi:10.1088/1361-6501/ac0333

†Corresponding author: jonathan.lemarechal@dlr.de

ture fluctuation between two consecutive TSP recordings is assumed to be proportional to the local skin friction velocity u_τ, which is related to the skin friction via the fluid density. This approach can only be applied in turbulent flow, where sufficient temperature fluctuations occur.

Besides the approach to derive skin friction from temperature measurement, only S3F (Fonov et al., 2005), shear sensitive liquid crystals (Klein and Margozzi, 1970; Gaudet and Gell, 1989), and luminescent oil-film flow-tagging (LOFFT) (Husen et al., 2017) provide direct spatial skin friction measurements. These also provide the direction of skin friction (Reda and Muratore, 1994; Fonov et al., 2005; Husen et al., 2017). In this paper a new approach to skin friction measurement based on TSP will be shown.

The TSP method relies on the temperature-dependent emission of fluorescent or phosphorescent light from temperature-sensitive luminophores. The luminophores are excited by light, which is typically in the UV-range. Then, the luminophores can return to their ground state by two main processes: a radiationless de-excitation (thermal quenching) or the emission of light. The emitted light is of a larger wavelength (Stokes shifted) and is typically in the range of visible light. With increasing temperature the radiationless de-excitation is more likely, which results in less emission. More details of the photophysics of TSP are provided by Liu and Sullivan (2005). For aerodynamic and hydrodynamic applications the luminophores are embedded in a clear coat. The acquisition system consists of a LED or laser of appropriate wavelength and a photosensitive device, e.g., a CCD or CMOS camera. Therefore, the TSP method is suitable for measurements in water in contrast to IR measurements due to the absorption of IR light by water (Buiteveld et al., 1994).

The TSP method is non-intrusive, because the coating can be integrated flush into the model surface and polished afterwards to the desired roughness. Because of the high density of luminophores in the clear coat the spatial resolution is determined by the camera and the optical setup. Each pixel of the acquired images corresponds to a single temperature probe, which results in a large number of probes with high density. The uncertainty of TSP temperature measurements was previously analyzed for super-sonic flows (Liu et al., 1995; Cattafesta et al., 1998). Factors contributing to the uncertainty of temperature measurements are given by Liu et al. (1995); Liu and Sullivan (2005). Their findings indicate that the image registration, which can be necessary due to model movement, model deformation or camera movement, is a major error source. It results in a change of the illumination pattern on the model and acquiring the same location on the model with different pixels, which makes the measurement susceptible to a variation of the gain. Further uncertainties are caused by the TSP calibration and the illumination and acquisition system.

In this paper the TSP method is used not only for temperature but also for skin friction measurement in a water facility. At first the Europium-based TSP in polyurethane PUR clear coat is characterized for quantitative temperature measurements in water. Additionally, the spatial temperature and skin friction distribution is measured in the wake of a single truncated cylinder, which is submerged in a laminar boundary layer. Furthermore, the skin friction distribution of an array of roughness elements, which were applied to delay the laminar-turbulent transition in a boundary-layer prone to Tollmien-Schlichting instability are investigated. For the quantitative TSP measurements an in-depth analysis of the measurement uncertainties and errors is presented.

2. Experimental methods

2.1. The laminar water channel

The experiments were conducted in the laminar water channel (Laminarwasserkanal) at the Institute of Aerodynamics and Gas Dynamics, University of Stuttgart. This facility was designed to provide a high flow quality suitable for experiments investigating the laminar-turbulent transition of two-dimensional boundary layers (Strunz, 1987). The velocity range of the facility ranges from 0.04 m/s to 0.2 m/s (Puckert et al., 2018). Due to the turbulence level of $Tu = 0.05\,\%$ in the frequency range of 0.1 Hz–10 Hz (Wiegand et al., 1995) and a fluid temperature variation below ± 0.05 K/day (Wiegand et al., 1995) the laminar water channel provides stable conditions and high repeatability.

In the test section of 10 m length and 1.2 m width a flat plate of 8 m length and 8 mm thickness is installed with an elliptic leading edge with an axis ratio of 10:1. The free water surface is 0.15 m above the flat plate surface. The flat plate is set up to achieve a close to zero pressure gradient, which results in the development of a Blasius-like boundary-layer flow. The flat plate and the test section are made of glass and provide great optical access. The boundary layer in the corner of the flat plate and the side walls of the test section is prone to instability. To avoid turbulent

flow contaminating the flat plate boundary layer the unstable flow in the corner is sucked to the lower side of the flat plate through a slit between the flat plate and the side walls of the test section. The necessary pressure difference between top and bottom side of the flat plate is generated by a screen at the end of the flat plate (Kruse and Wagner, 1998).

2.2. Experimental Setup

Two types of roughness elements were used to generate a disturbance of the laminar flow to achieve a stationary skin friction distribution. Their location are shown in fig. 1, which also defines the coordinate system. The conditions in the laminar water channel require placing a TSP coated thin structure with an integrated model heating onto the fixed flat plate. This structure was made from fiber reinforced plastic and is referred to as TSP element (Lemarechal et al., 2019). The size of the TSP element is $(x \times z) = (1.085\,\mathrm{m} \times 1.00\,\mathrm{m})$.

The first application is a simple experimental setup consisting of a short cylinder, which is submerged in the laminar boundary layer. The cylinder has a diameter of $d_c = 15\,\mathrm{mm}$ and a height of $k = 5\,\mathrm{mm}$. As shown in fig. 1a, it is located at the upstream end of the TSP element at $x = 3.218\,\mathrm{m}$. The field of view (FOV) of the TSP measurement and the location of the measurement plane of the hot-film (HF) anemometry measurement is indicated in fig. 1.

In the second test, the TSP method is applied to determine the skin friction around an array of roughness elements from the temperature distribution. These roughness elements are of cuboid shape with a length of $l = 13.3\,\mathrm{mm}$, a width of $w = 3.5\,\mathrm{mm}$, and a height of $k = 6.5\,\mathrm{mm}$. The elements are arranged with an angle of 45° to the flow direction. The complicated flow field around the roughness elements is dominated by vortices (Groskopf et al., 2011; Lemarechal et al., 2018). These vortices induce large velocity gradients in proximity of the surface, which prohibits velocity measurements for comparison, because of spanwise velocity components, which would not be possible to acquire with the current hot-film setup.

2.3. Measurement techniques

2.3.1 Temperature-Sensitive Paint method

The TSP method was previously applied in the same laminar water channel for time-resolved surface-based flow visualizations of a flat-plate boundary layer at the late stage of laminar-turbulent transition (Lemarechal et al., 2018, 2019). In the following the TSP measurement system, which consists of the TSP element and the acquisition system, are explained in detail. Furthermore, the data evaluation is presented.

The TSP element is partially coated ($x \times z = 1.00\,\mathrm{m} \times 0.25\,\mathrm{m}$) with a Europium-based TSP (Ondrus et al., 2015). For this TSP the high temperature sensitivity ($-3.3\,\%/\mathrm{K}$ at $20\,°\mathrm{C}$) and negligible pressure-sensitivity are characteristic. Besides the surface coating with TSP an integrated electrical model heating, which has a width of $0.30\,\mathrm{m}$, is integrated in the TSP element. The heating is a resistance heating based on a single current-carrying layer of carbon fiber. To minimize the disturbance of the boundary-layer flow by the TSP element the thickness is minimized in the design process. A total thickness of $1.9\,\mathrm{mm}$ is achieved. Thus, the TSP element thickness d normalized by the displacement thickness δ_1 is approximately $d/\delta_1 = 0.21$.

The acquisition system consists of two LEDs (HARDsoft IL-105/6X Illuminator UV) and one scientific black-and-white CCD camera (pco.4000). The camera and LEDs are placed above the test section to illuminate the TSP and record the emission of the TSP through the free water surface. This setup makes the TSP measurement susceptible to measurement errors caused by disturbances of the free water surface like surface waves, which is discussed in section 5. Optical filters were installed on the camera (center wavelength $630\,\mathrm{nm}$; bandwidth $75\,\mathrm{nm}$) and LEDs (center wavelength $385\,\mathrm{nm}$; bandwidth $70\,\mathrm{nm}$) to reduce the amount of stray light and thus improve the signal-to-noise ratio. The camera recorded images with $10\,\mathrm{Hz}$ at an exposure time of $4.5\,\mathrm{ms}$. The optical setup of the camera results in an image resolution of approximately $4.4\,\mathrm{px/mm}$. The acquisition method used was the so-called intensity method (Liu and Sullivan, 2005). Therefore, the LEDs were operated in the continuous wave mode. The peak emission is at $\lambda \approx 405\,\mathrm{nm}$ with an output light power of approximately $3.5\,\mathrm{W}$ each.

The TSP acquisition sequence consisted of four phases, i.e., the dark, reference, heat-up, and run phase. At first 10 images without illumination by the LEDs were acquired in the dark phase to record the background light. Secondly, 100 images with illumination are recorded, when the TSP surface and the fluid are in temperature equilibrium. Afterwards, the LEDs are switched off and the electrical heating is switched on at constant electrical heating power P_{el}.

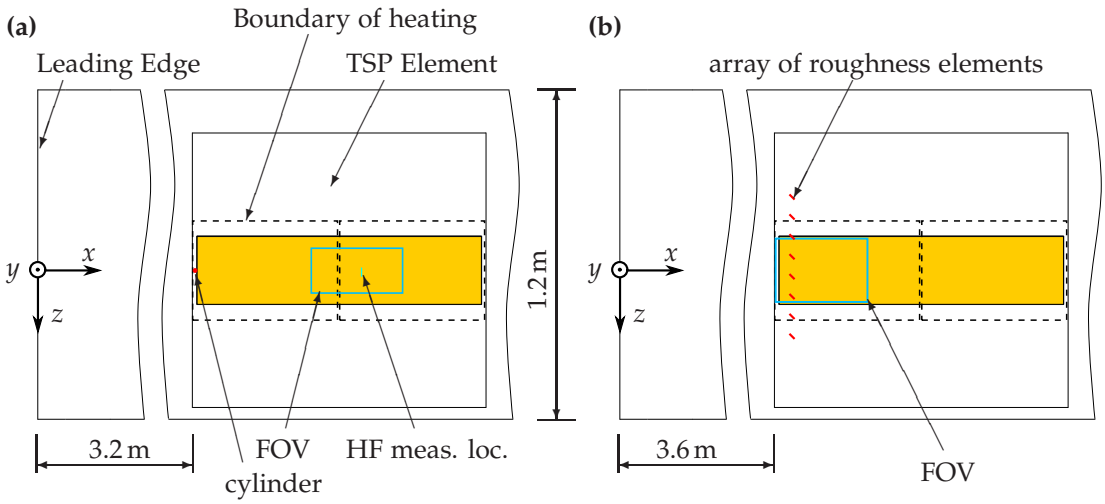

Figure 1: *Top view of the experimental setups:* ***a*** *short cylinder and* ***b*** *spanwise array of cuboid roughness elements. Also, the coordinate system is defined.*

The heat-up phase lasts several minutes until a constant surface temperature is reached. Finally, the run phase is started and 900 images are recorded with constant heat flux $\dot{q}$ between TSP element and fluid. The recorded intensities of the dark, reference, and run phase are labeled I_{dark}, I_{ref}, and I, respectively.

The first steps of the data evaluation were performed with a software developed by DLR, called *nToPas* (Klein et al., 2005). At first the images of each phase are averaged over time. Subsequently, the averaged dark image is subtracted from the averaged reference and run images. Then, the result image is calculated by dividing the averaged reference image by the averaged run image. Finally, the resultant image with the intensity ratio $\bar{I}_{ref}/\bar{I}$ is mapped onto a structured surface grid of 1 mm-by-1 mm resolution. For each grid point 3 px-by-3 px are averaged.

The surface temperature T during the run phase can be derived from measured intensities at reference and run phase conditions with the Arrhenius equation (Liu et al., 1995)

$$\ln \frac{I(T)}{I(T_{ref})} = \frac{E_{nr}}{R}\left(\frac{1}{T} - \frac{1}{T_{ref}}\right). \tag{1}$$

Besides the temperature at reference conditions T_{ref} the activation energy E_{nr} and the universal gas constant R is needed. A simplified empirical equation is used, because the activation energy E_{nr} proves to be difficult to measure (Liu and Sullivan, 2005):

$$T - T_{ref} = \frac{1}{S} \ln\left(\frac{I_{ref}}{I}\right) \tag{2}$$

The necessary temperature sensitivity S of the TSP coating is derived from calibration measurements with TSP samples as described by Egami et al. (2009). Since, the reference images were recorded at the known fluid temperature T_∞, these are used to apply the calibration.

2.3.2 Skin friction measurement

Since, momentum transport and thermal transport are related, their dependency can be described empirically with the Reynolds analogy for $\mathrm{Pr} \approx 1$ (Reynolds, 1874) and the Colburn analogy for $\mathrm{Pr} \neq 1$ (Colburn, 1933; Lin, 1994). The Colburn analogy correlates the local skin friction coefficient C_f to the Nusselt number Nu, Reynolds number Re and Prandtl number Pr:

$$\frac{\mathrm{Nu}}{\mathrm{RePr}^{1/3}} = \frac{C_f}{2} \tag{3}$$

This empirical relation relies on the assumption of the same onset of the momentum and thermal boundary layer and also a uniform heat flux. Furthermore, it is limited to simple flow configurations, such as laminar forced convection (Lin, 1994). This excludes flows with flow separation (Rudolph, 2011) and form drag (Lin, 1994). A successful application of the Reynolds analogy for skin friction measurement was demonstrated by Rudolph (2011) for a steady, laminar flat-plate flow and a laminar flat-plate flow disturbed by a trip wire.

The experimental setup at the laminar water channel, where the thermal boundary layer begins significantly later than the momentum boundary layer, requires to adapt the Colburn analogy. Thus, a formu-

lation of the Colburn analogy with a later beginning x_0 of the thermal boundary layer is used (Cebici and Bradshaw, 1984):

$$\mathrm{St} = 0.322 \cdot \mathrm{Re}^{1/2}\mathrm{Pr}^{2/3}\left[1-\left(\frac{x_0}{x}\right)^{\frac{3}{4}}\right]^{-\frac{1}{3}}, \qquad (4)$$

with the Stanton number St. To actually calculate the local skin friction τ_W the following equation is used:

$$\tau_W = \frac{\dot{q}_W U_\infty}{(T_W - T_\infty)}\frac{Pr^{2/3}}{c_p}\left[1-\left(\frac{x_0}{x}\right)^{\frac{3}{4}}\right]^{-\frac{1}{3}}. \qquad (5)$$

Hence, a heat flux $\dot{q}_W$ between the wall and the fluid, which is caused by the temperature difference between the wall T_W and the fluid, is necessary. In addition, the freestream velocity U_∞ and the specific heat capacity at constant pressure c_p of the fluid are needed. The electrical heating power $\dot{q}_{el}$ is not a suitable input for the heat flux $\dot{q}_W$ because of unknown losses in the cables and to the underside of the TSP element, which is not insulated. An approach to determine $\dot{q}_W$ is necessary because the TSP element is not equipped with any possibility to directly measure $\dot{q}_W$. The local skin friction of the Blasius boundary layer and the measured surface temperature are used in (5) to determine $\dot{q}_W$. This approach is justified because the flow in the laminar water channel is in good agreement with the Blasius boundary layer, i.e., the deviation of the shape factor H_{12} is approximately 15 % in the presence of the forward-facing step at the leading edge of the TSP element, which is slightly worse than in previous experiments in the same facility (Wiegand et al., 1995; Subasi et al., 2015). This approach enables to measure the deviation of the skin friction from that of the Blasius boundary layer, which is of interest for the tested setups.

2.3.3 Hot-film anemometry

Hot-film anemometry measurements were performed to supply reference data for the TSP evaluation. The single-wire hot film (Dantec 55R15) was operated in constant temperature mode with a wire-to-fluid temperature ratio of 1.08. The probe signal was recorded at 100 Hz over 30 s. Before the measurement the probe was calibrated by moving the probe with the traversing system at 20 different speeds through the test section, when the fluid is at rest (Subasi et al., 2015).

The hot-film anemometry was used to measure velocity profiles in the yz-plane in the wake of the cylindrical roughness element as indicated in fig 1a.

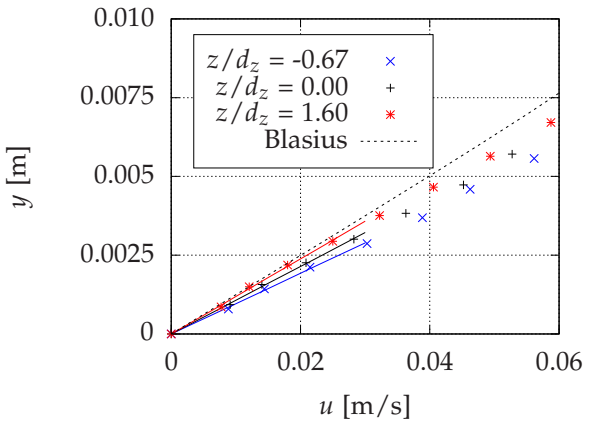

Figure 2: *The velocity profiles close to the wall are shown for the Blasius boundary layer, the undisturbed boundary layer(z/d_z = 1.60), the maximum skin friction (z/d_z = -0.67), and minimum skin friction (z/d_z = 0.00) in the wake of the roughness element.*

Over a span of $\Delta z = 40$ mm a vertical velocity profile was measured every 2 mm. Each profile consists of 20 measurements from $y = 1$ mm to $y = 30.2$ mm. For each wall normal velocity profile $u(y)$ the wall shear stress is derived from the velocity gradient at the wall $\partial u/\partial y|_{y=0}$. The velocity measurements below $y = 7$ mm are shown in fig 2 for different spanwise locations behind the roughness element. The result indicates that the velocity gradient close to the wall is well resolved and in better agreement with the Blasius boundary layer than the previously mentioned shape factor H_{12}. The hot film measurements were performed with the same setup as the TSP measurements except for the artificial heat flux between model and flow, which was switched off for the hot-film measurements.

3. Temperature-sensitive paint in water

In the following, a characterization of TSP exposed to water for longer time is presented, because it is well known, that water diffuses into PUR. The PUR used for the TSP coating reaches a water content of 24 g/kg after storing a sample in water for two days. The water content could lead to an alteration of the characteristics of the TSP, which could be similar to aging effects of TSP like photodegradation (Liu et al., 1995). Thus, the stability of the measurable emission and the temperature sensitivity of waterlogged TSP are investigated to assess the influence of the PUR wa-

ter content on temperature measurements with TSP in water. The tests were conducted with tap water and a maximum water height of 0.15 m.

3.1. Reduction of emission in water

The first applications of TSP in water already showed a reduction of the measurable emission when the models were placed in water. This observation is further investigated in the laboratory. The calibration chamber for TSP and PSP at DLR (Egami et al., 2009) was upgraded to test one TSP sample in water and one reference sample in air synchronously. This setup enables to control the temperature and pressure of the samples. At $t = 0$ one sample is placed in water and the emission of both samples is recorded. At $t \approx 49\,\mathrm{h}$ the sample is removed from the water and the measurement is continued.

Figure 3 shows the emission, which is normalized by the emission at $t = 0$, of both samples over time for a constant sample temperature. Until $t = 48\,\mathrm{h}$ the emission of the sample in water is reduced by 15 %. This reduction of emission is significantly larger than the fluctuations of the reference sample in air. After removing the waterlogged sample from the water the emission increases again, as can be seen in fig. 3. A jump in the intensity ratio can be observed at $t \approx 49\,\mathrm{h}$ when the water is removed, which removes the damping of the light traversing the water.

To exclude that water influences the TSP luminophores a Jasco FP-6500 Spectrofluorometer was used to measure the absorption and emission spectra before and after placing a sample in water for two days. The measurement preparation after storing the sample in water consisted only of drying the surface; therefore, the TSP was still waterlogged. The comparison of the normalized spectra revealed that exposing the TSP to water does not significantly influence the shape of the spectra or the ratio of absorption to emission peak. These results indicate that the TSP luminophores are not influenced by exposing the TSP to water.

Another mechanism, which could influence the emission of the TSP, are changing optical properties of the clear coat. The applied TSP uses a PUR clear coat. Therefore, object plates for microscopy applications made from glass were coated with the PUR clear coat with and without TSP luminophores in different thicknesses. An Ocean Optics Miniature Spectrometer FLAME-S-UV-VIS in combination with a white light source were used to measure the transmission of dry and waterlogged PUR samples. The spectrometer is directly pointed at the light source and the respective sample is placed in between. Also, one reference sample, which is an uncoated glass substrate, was measured.

The transmission properties (fig. 4) of the glass substrate show that in the wavelength range relevant for the TSP ($350\,\mathrm{nm} \leq \lambda \leq 700\,\mathrm{nm}$) the transmission is approximately 90 %. The dry, pure PUR absorbs all light below 385 nm. For larger wavelengths the transmission increases and reaches a level of approximately 80 % to 85 %. A second dry PUR sample with a different thickness does not show significantly different transmission characteristics. When TSP luminophores are added to the PUR, the wavelength at which the transmission increases is shifted to larger wavelengths of approximately 420 nm. The sample reaches a transmission of up to 80 % except for one peak, which coincides with the emission peak of the applied TSP. These two observations show the absorption and emission of light by the TSP luminophores. The emission at longer wavelength is called Stokes shift, which can be observed in the setup due to the white light source used for the transmission measurement.

In the second step two PUR samples were stored in water for two days. After drying the surface the transmission spectra measurements were repeated. Both samples show a reduced transmission over the entire wavelength range but the largest reduction is observed for wavelengths below 450 nm. This coincides with the wavelength range necessary to excite the TSP luminophores. Also, at the wavelength of the emission of the luminophores, i.e. at approximately 615 nm, the transmission is reduced. These changes are significantly larger than the variation of transmission observed for the repeated measurement of the dry sample.

It is observed that the optical properties of the PUR change when water diffuses into the PUR clear coat of the TSP. Water in the PUR reduces the transmission of light for the wavelength relevant for excitation and emission of the TSP. When placing a TSP coated model with a dry TSP coating into water the reduction of the transmission of light starts. Thus, reference and run images acquired during the time span of the gradual reduction of the transmission will contain additional intensity reduction. The findings indicate that for the acquisition timing at the laminar water channel a temperature measurement error of 0.07 K can be caused at the beginning of a measurement. Furthermore, these findings are in agreement with the observations made during experiments that

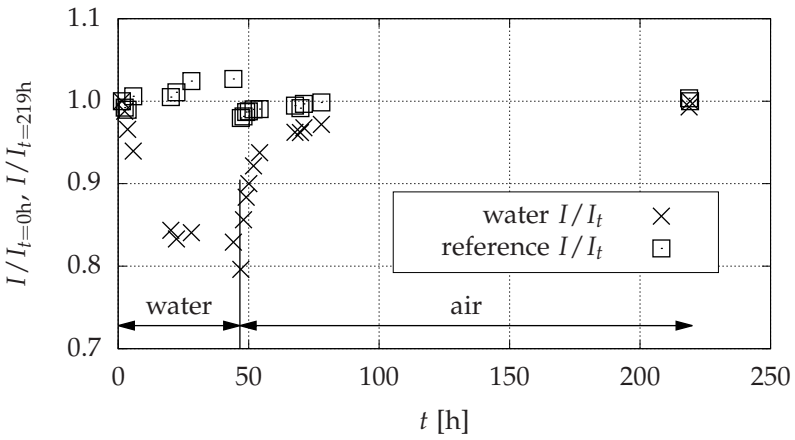

Figure 3: *Measurable emission of a TSP sample placed into water for $t \approx 49$ h and a reference sample in air.*

the recorded emission decreases at the beginning of measurements, when the model was just put in water.

3.2. Temperature sensitivity in water

The temperature sensitivity of waterlogged TSP is investigated by means of three TSP coated samples. These were calibrated in the DLR calibration chamber with a limited temperature and reduced waiting time to avoid an influence of changing optical properties of the PUR clear coat. Reducing the waiting time was necessary to limit the influence of the steep change of emission by the drying samples (see fig. 3) on the calibration. After placing two samples in water for 80.6 h the samples' surface was dried and two more calibrations were conducted 0.33 h and 14.75 h after removing them from water. Figure 5 shows the temperature dependent intensity and normalized intensity. The development of the intensity in fig. 5a reflects the results from fig. 3 that a sample with higher water content shows a reduced emission. Despite the reduced emission the normalized intensity of the dry and waterlogged samples in fig. 5b coincide. From these calibrations the temperature sensitivity for each sample is derived and listed in table 1. When the temperature sensitivity of the samples is compared for each calibration individually, the dry and waterlogged TSP samples show only small deviations of the temperature sensitivity. However, the first calibration after removing the samples from water deviates from the other calibrations. It is expected that reduced waiting times, which are necessary to avoid a significant change of the water content during the image acquisition, could lead to a sample temperature which has not reached its equilibrium.

t [h]	S_{ref} [% K^{-1}]	S_1 [% K^{-1}]	S_2 [% K^{-1}]
before	-3.5	-3.5	-3.5
0.33	-3.7	-3.7	-3.6
14.75	-3.6	-3.5	-3.5

Table 1: *Temperature sensitivity S (at $T_{ref} = 18$ °C) for a reference sample S_{ref} and two samples with varying water content of the clear coat.*

4. Results and discussions

4.1. Truncated cylinder

The TSP visualization of the wake of the truncated cylinder is shown in fig. 6. In the figure the flow is from left to right and the cylinder is located upstream of the FOV. The visualization shows two parallel areas of lower intensity ratio, which are oriented in streamwise direction, at ($|z/d_c| < 2$). These are caused by a horseshoe vortex which is induced by the truncated cylinder (Gregory and Walker, 1956). The TSP visualization shows that the wake of the cylinder is laminar, which is indicated by the absence of thermal fluctuations in the wake as previously observed for transitional and turbulent wakes of truncated cylinders (Lemarechal et al., 2020). This is also supported by the low roughness Reynolds number of $\mathrm{Re}_{kk} = u_{(y=k)}k/\nu = 177$ (Gregory and Walker, 1956; Sedney, 1973). The visualization also shows an area of low intensity ratio across the flow direction. This is caused by a gap in the heating, which is indicated in fig. 1a.

For each of the different heating power density settings ($\dot{q}_{el} = 267$, 400 and 533 W/m^2) the measured in-

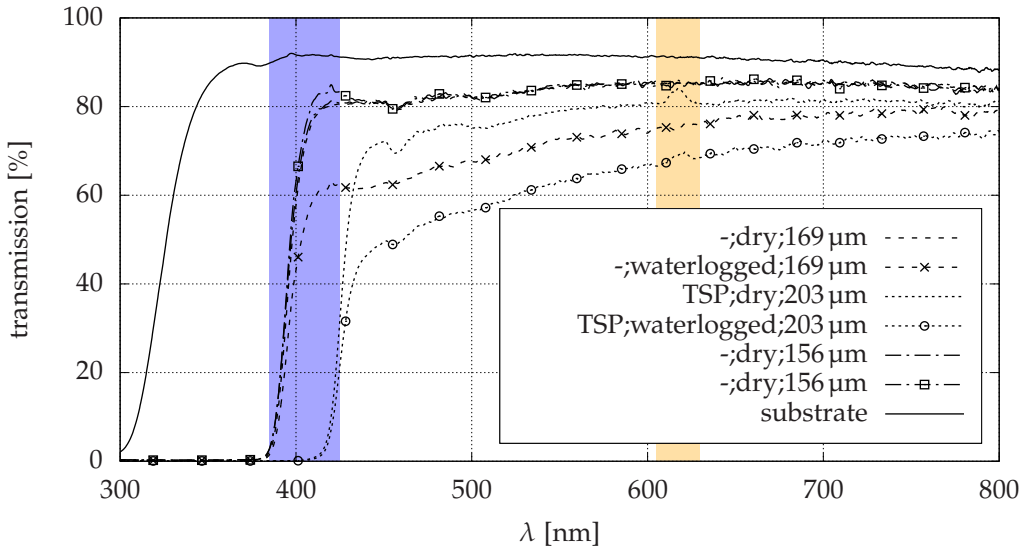

Figure 4: *Transmission characteristics of the PUR clear coat for three different samples and different conditions. Also, the transmission characteristics of the glass substrate is shown and the wavelength range relevant for excitation* ($385\,\mathrm{nm} \leq \lambda \leq 425\,\mathrm{nm}$) *and emission* ($605\,\mathrm{nm} \leq \lambda \leq 630\,\mathrm{nm}$) *of the TSP are highlighted in blue and orange, respectively.*

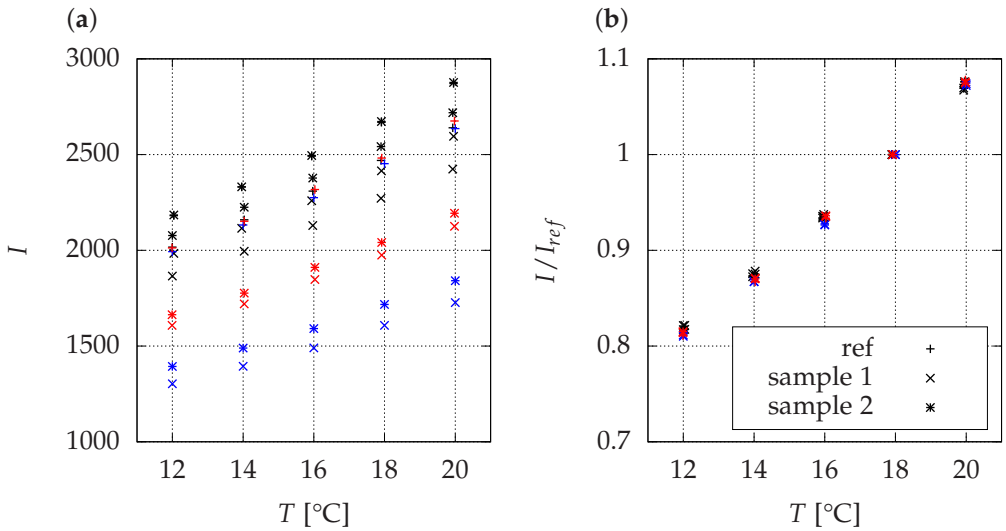

Figure 5: ***a*** *Temperature dependent intensity I and* ***b*** *the normalized intensity of the TSP for different conditions: (black) before placing the samples in water for* 80.6 h *and (blue)* 0.33 h *and (red)* 14.75 h *after removing the samples from water.*

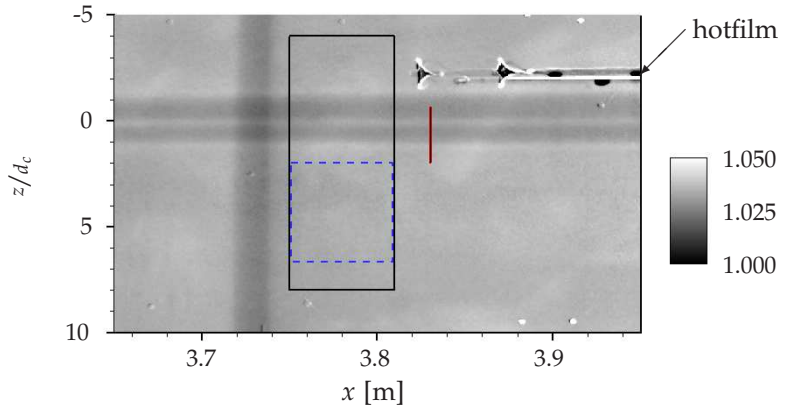

Figure 6: *TSP visualization of the cylinder wake. The location of the hot-film measurement (—), the area to evaluate the heat flux density $\dot{q}_W$ (– –), and the area in which the skin friction is derived from TSP data (—) are indicated.*

tensities are averaged in streamwise direction in the area indicated in fig. 6. Equation 2 is used to derive the surface temperature from the intensity ratio for each heating power setting shown in fig. 7. The heating power $\dot{q}_{el} = 400\,\mathrm{W/m^2}$ was performed for two fluid temperatures T_∞, which differed by 0.1 K. The resulting surface temperature differs already significantly. Increasing the heating power density $\dot{q}_{el}$ increases the temperature difference between the minima and the maximum as well as the difference between the minima and the continuous value of the undisturbed laminar flow. In the wake of the truncated cylinder ($|z/d_c| < 2$) two symmetric minima at $z/d_c = \pm 0.55$ with a local maximum directly downstream of the cylinder ($|z/d_c| = 0$) are visible in the intensity ratio in fig. 7. Outside of the wake the intensity ratio and temperature reach a constant value, as it is expected for an undisturbed laminar boundary layer. The comparison of the local maximum and the undisturbed boundary layer shows that the maximum does not reach the same value as the undisturbed boundary layer. Increasing the heating power increases the intensity ratio $\bar{I}_{ref}/\bar{I}$ in the undisturbed boundary layer as well as in the wake of the cylinder.

Figure 6 also shows the area used to evaluate the heat flux $\dot{q}_w$ and the temperature. Within these areas a significant intensity gradient in flow direction is not visible; therefore, the intensities are averaged in streamwise direction. The heat flux density $\dot{q}_W$ is estimated with the assumption that the undisturbed laminar flow can be represented by the Blasius boundary layer. The average temperature in the area $x = 3.75\,\mathrm{m} - 3.81\,\mathrm{m}$ and $z/d_c = 2 - 7$ (fig. 6) and the local skin friction of the Blasius boundary layer for $x = 3.81\,\mathrm{m}$ are used to calculate $\dot{q}_W$ with (5). Table 2 lists for each tested electrical power density the associated heat flux density. It stands out that only 14.9 % – 17.6 % of the electrical power density constitutes the heat flux density.

$\dot{q}_{el}$ [$\mathrm{Wm^{-2}}$]	$\dot{q}_W$ [$\mathrm{Wm^{-2}}$]	T_∞ [°C]
267	46.0	17.9
400	66.6	17.8
400	59.4	17.9
533	93.8	17.9

Table 2: *Electrical heat flux density $\dot{q}_{el}$, as adjusted on the power supply, and the determined effective heat flux density $\dot{q}_w$.*

The determined heat flux density is assumed to be constant in spanwise direction and is used to calculate the skin friction with (5) from the temperature profile in fig. 7. The absolute values of the skin friction profiles are in good agreement for the tested heat flux densities, see fig. 8. Only the absolute of the maxima deviates for the lowest heating power. Therefore, it is concluded that the design of the heating provides good repeatability even when changing the heat flux. In fig. 8 also the skin friction results of the velocity measurement are shown. The TSP results are in good agreement with the hot-film results, especially the maximum at $z/d_c = -0.4$ and the minimum at $z/d_c = 0$. A deviation between TSP and hot film is visible at $z/d_c > 0$. These are very likely caused by the measurement procedure, i.e., profiles were measured beginning close to the wall and traversing upward beginning on the negative z-side. The long measuring time reduces the applicability of the calibration. Nevertheless, deriving the heat flux in a region

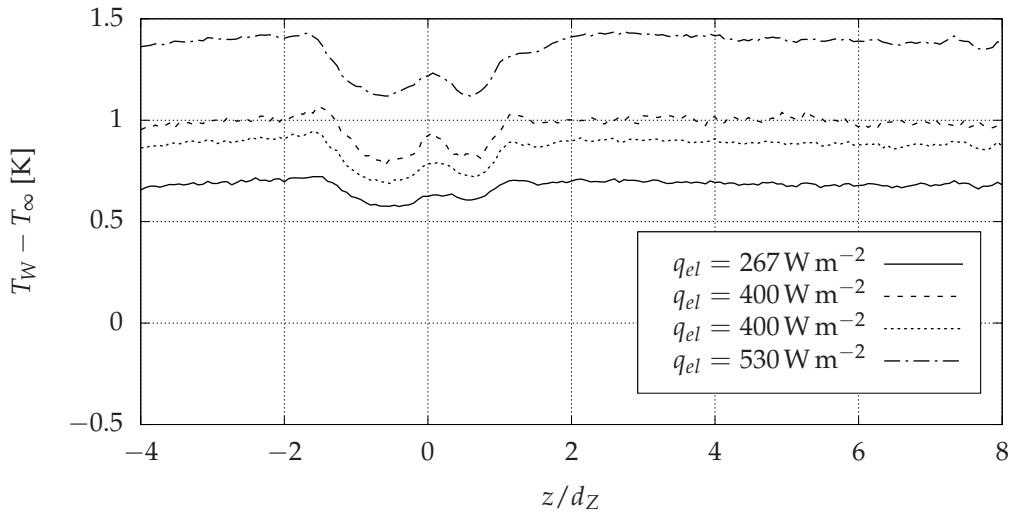

Figure 7: *Temperature distribution 37.5 roughness heights downstream of the truncated cylinder.*

uninfluenced by the roughness elements is suitable for the laminar water channel. The uncertainty of the skin friction determined from the velocity measurement is estimated and the errorbars are shown in fig. 8. The relative uncertainty is approximately 10 % and dominated by the position accuracy of the traversing system.

The conditions of the TSP measurement at the laminar water channel, i.e., the measurement equipment, the stable reference condition provided by the facility, averaging 900 images, and averaging several grid points in flow direction, results in a temperature resolution of $(\Delta T)_{min} < 0.007\,\mathrm{K}$ (Liu and Sullivan, 2005). The minimum detectable difference in skin friction is calculated for each heat flux density: $(\Delta\tau)_{min} = 1.96$, 2.69, and $4.01 \times 10^{-5}\,\mathrm{N/m^2}$. These are below 1 % of the local skin friction of the laminar boundary at the measurement location.

4.2. Array of oblique roughness elements

Hereafter, the absolute skin friction of the near field of an array of roughness elements is analyzed. To apply (5) for this boundary condition an effective heat flux $q(x)$ is determined from $x = 3.3\,\mathrm{m}$ to $4.2\,\mathrm{m}$ in areas uninfluenced by the roughness elements. This procedure is necessary to compensate the beginning thermal boundary layer.

Figure 9 shows the determined skin friction field. Three distinctive disturbances of the laminar flat plate flow can be observed: a horseshoe vortex (HV), a trailing edge vortex (TV), and a leading edge vortex (LV). The horseshoe vortex and the trailing edge vortex increase the skin friction by a factor of two compared to the undisturbed boundary layer. The maximum skin friction caused by the leading edge vortex varies significantly in contrast to the other vortex types. A systematic influence of the roughness elements on the measured skin friction by a possible change of the heat flux of the roughness elements made of brass cannot be detected.

Despite the three-dimensional nature of the flow, only minor flow separation occurs. Therefore, the proposed method to derive the skin friction field is still applicable to the measured temperature field but a reduced accuracy has to be expected. The TSP method provides a method which is fast in acquisition and data reduction to initially evaluate the effectiveness of drag reduction methods such as methods delaying the laminar-turbulent transition, e.g., spanwise mean velocity gradients technique (Fransson et al., 2005), and upstream flow deformation (Wassermann and Kloker, 2002). Hence, the net gain of the drag reduction methods could be estimated from large-area skin friction fields measured with TSP.

5. Uncertainty Analysis

Hereafter, the bias and precision errors contributing to the temperature and skin friction measurement with TSP are discussed. Furthermore, the TSP element or the necessary heat flux could alter the flow (Lemarechal et al., 2019). These issues are of minor importance for the evaluation of TSP for quantitative temperature or skin friction measurements in water

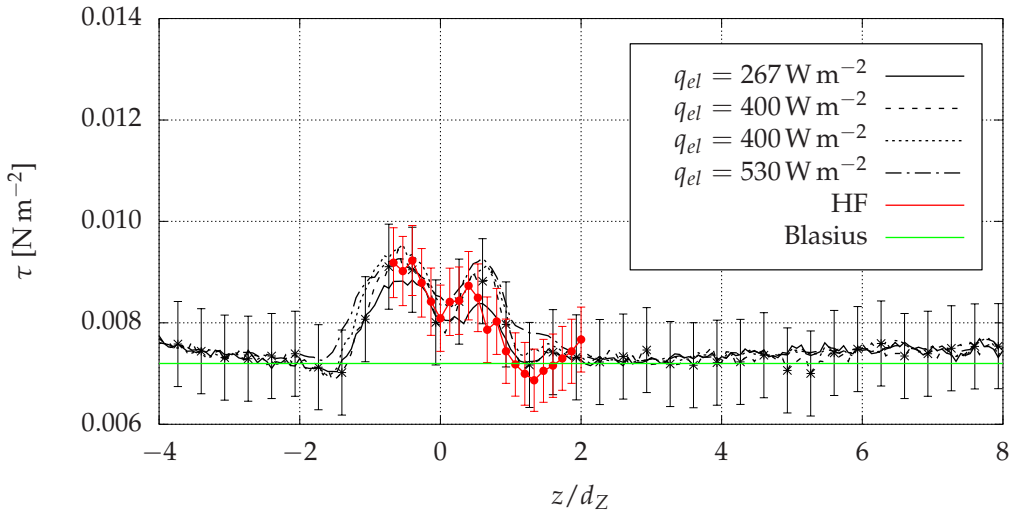

Figure 8: *Skin friction derived from TSP and hot-film measurements 37.5 roughness heights downstream of the truncated cylinder. The uncertainty of the TSP measurement is derived in section 5.*

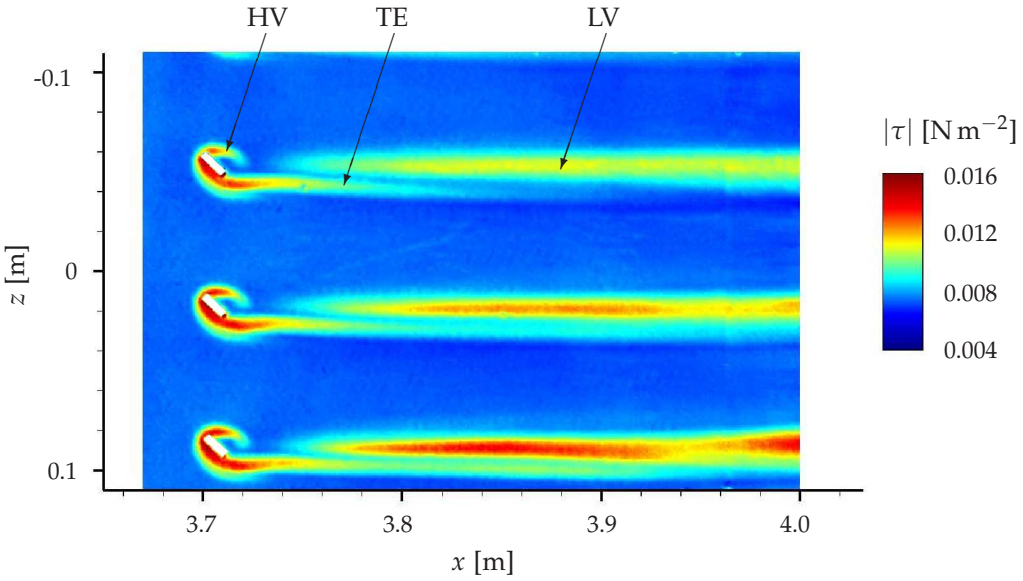

Figure 9: *Skin friction field in the near field of an array of roughness elements.*

and therefore not further discussed.

From the uncertainty analysis of Liu et al. (1995) and Cattafesta et al. (1998) it can be concluded that relative motion between the acquisition system, i.e. the camera and LED, and the model is a key contributor to the temperature uncertainty. Besides the mechanisms causing changes in the optical path mentioned by Liu et al. (1995) and Cattafesta et al. (1998), i.e., model movement, model deformation, and movement of the acquisition system, another contributor can occur in the laminar water channel, i.e., surface waves.

Since, the movement of the camera system can be neglected, because of the minuscule vibrations of the facility, the camera system can be used to quantify the model movement and influence of possible surface waves. The evaluation of the distance between each marker in the first reference image and all following reference and run images of the same data point for 24 data points, i.e., 21000 images, shows that the movement is smaller than 2 px (0.5 mm) with 50 % of the displacements in the order of 0.5 px (0.125 mm). These variations are significantly smaller than the structures caused by the roughness elements. Therefore, image registration during the evaluation and errors caused by changes of the optical path are neglected. Hence, the overall uncertainty of the temperature and skin friction measurement is composed of the uncertainty analysis of the TSP calibration, the camera and the LED.

5.1. Calibration

The temperature sensitivity of the applied TSP is not affected by water, as ascertained in section 3. Therefore, the uncertainty of the calibration was determined in the DLR calibration chamber (Egami et al., 2009) with synthetic air as the working gas. Eleven calibrations with an unaltered setup were conducted on ten consecutive days. The calibrations were limited to the temperature range relevant for the laminar water channel (12 °C to 24 °C).

The Arrhenius diagram in fig. 10a already shows a very good agreement with small standard deviation. Since, the temperature range is limited the temperature deviations from the determined calibration curve are small as shown in fig. 10b. Thus, the standard deviation of the calibration of 0.13 K contributes to the precision error. This standard deviation is small in comparison to the results of other performed calibration uncertainties (Liu and Sullivan, 2005).

Table 3: *Camera settings and parameter of the pco.4000 (PCO AG, 2004) relevant for the measurement uncertainty.*

parameter	variable	unit	value
dynamic range AD	n_{bit}	bit	14
exposure	t_{exp}	ms	4.5
readout noise	N_{read}	e^-	14
FWC	C_{FW}	e^-	60000
dark current	I_d	$e^-/(s\,px)$	0.02

5.2. Acquisition system

First, the precision error of the intensity measurement is quantified. Three types of noise, which are determined by the camera type and the camera settings, are considered: photon shot noise P_{shot}, dark current P_{dark}, and readout noise P_{read}. In table 3 the settings relevant for the uncertainty analysis of the pco.4000 camera are listed. Furthermore, an intensity of $I = 12.500$ counts is assumed. The three types of noise can be calculated according to Cattafesta et al. (1998) as follows:

$$P_{shot} = \frac{2}{\sqrt{I}} = 0.018, \tag{6}$$

$$P_{dark} = \frac{2 I_d 2^{n_{bit}} t_{exp}}{C_{FW} I} = 3.9 \cdot 10^{-9}, \tag{7}$$

$$P_{read} = \frac{2 N_{read} 2^{n_{bit}}}{C_{FW} I} = 6.1 \cdot 10^{-4}, \tag{8}$$

with the dark current I_d, dynamic range of the analog-to-digital (AD) converter n_{bit}, full-well capacity (FWC) C_{FW}, and the readout noise N_{read}.

Besides the precision error the camera is also prone to bias error due to non-linearities of the analog-digital converter $B_{linear} = 2/I$ and the resolution of the AD converter $B_{Res} = 0.5/I$.

The illumination by LEDs causes uncertainties due to changing characteristics with increasing LED temperature, i.e., a shift of the emission peak and decrease of radiant flux. Heating the surface with the radiation of the LED is not expected to be relevant for the setup at the laminar water channel due to the large amount of water and the good heat transfer. The two LED systems (HARDsoft IL-105/6X Illuminator UV) were operated at the maximum forward current of 18 A, which results in significant heating of the LED chip. In the applied HARDsoft LED system a LED chip of the type Luminus UV CBT-120-UV (Luminus Devices, Inc., 2016) is installed. A temperature change of 80 K shifts the emission peak by approximately 5 nm (Luminus Devices, Inc., 2016), which does not cause a significant change in the excitation characteristics of the applied TSP coating. However,

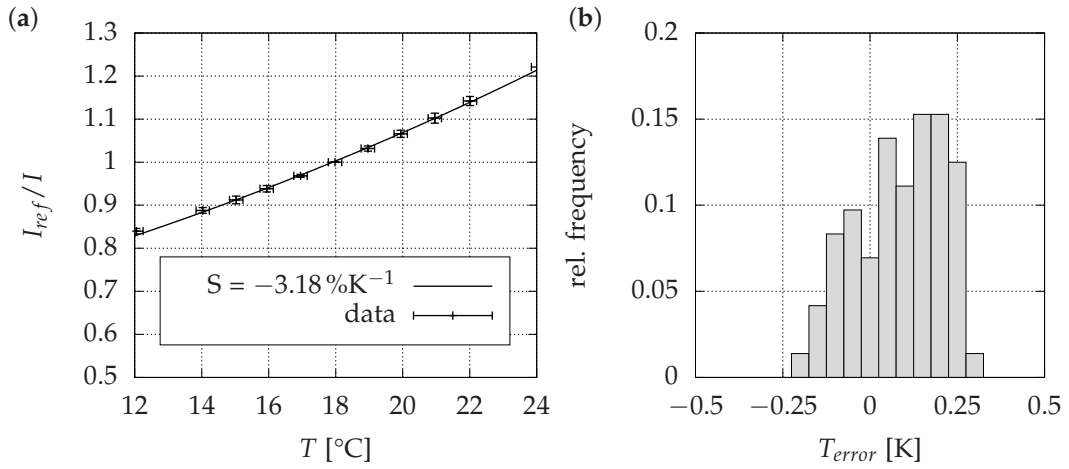

Figure 10: *a) Arrhenius diagram with errorbars (exaggerated by factor 2), which represent the standard deviation of the intensity ratio and the temperature error of the calibration chamber. b) the relative frequency of the deviation from the calibration of the applied TSP.*

the temperature increase reduces the radiant flux of the LED causing a bias error of the LED ($B_{LED} = 0.01$). The fluctuations of the LED are estimated to result in a precision uncertainty of $P_{LED} = 0.002$.

5.3. Uncertainty temperature measurement

The bias error $B_{\Delta T}$ of the TSP temperature measurement is calculated with (Cattafesta et al., 1998):

$$B_{\Delta T}^2 = \left(\frac{1}{S}\right)^2 \left[2\left(B_{Gain}^2 + B_{linear}^2 + B_{Res}^2\right) + B_{Motion}^2 + B_{LED}^2\right] \tag{9}$$

As a result of the negligible motion of the model and acquisition system the bias error caused by the pixel-to-pixel gain variation B_{Gain} and the relative motion B_{Motion} are assumed to be $B_{Gain} \approx B_{Motion} \approx 0$. The resulting bias of the temperature measurement is $B_{\Delta T} \approx 0.29\,°C$, which is dominated by the reducing radiant flux of the LED.

Furthermore, the precision error is determined $P_{\Delta T}^2$, which is also calculated following Cattafesta et al. (1998):

$$P_{\Delta T}^2 = \frac{1}{n}\left[2\left(\frac{1}{S}\right)^2 \left(P_{LED}^2 + P_{dark}^2 + P_{shot}^2 + P_{read}^2\right) + \Delta T_r P_k^2\right] \tag{10}$$

The precision error is small due to the large number of acquired images ($n = 900$) $P_{\Delta T} \approx 0.03\,°C$.

The total uncertainty $U_{\Delta T}^2$ of the TSP temperature measurement is calculated with

$$U_{\Delta T}^2 = B_{\Delta T}^2 + P_{\Delta T}^2 \tag{11}$$

(Cattafesta et al., 1998) and a value of $U_{\Delta T} \approx 0.3\,°C$ is determined. Hence, the total uncertainty is dominated by the decreasing radiant flux of the LED.

5.4. Uncertainty skin-friction measurement

The uncertainty of the TSP skin friction measurement for the presented test case of a truncated cylinder submerged in a laminar boundary layer (see section 4.1) is analyzed with the propagation of uncertainty. The Taylor series of (5) is derived and the determined uncertainty of the TSP temperature measurement together with the uncertainties listed in table 4 are used to calculate the uncertainty of the TSP skin friction measurement. Since the heat flux $\dot{q}_W$ is derived from the temperature measured with TSP and the skin friction of the Blasius boundary layer the bias $B_{\Delta T}$ of the TSP temperature measurement is not relevant for the uncertainty analysis. The result of the uncertainty analysis is $\pm 8.4 \times 10^{-4}\,N/m^2$ (approx. $\pm 10\,\%$).

The measurements with the Reynolds analogy by Rudolph (2011) showed an uncertainty in the order of 5 %. In this work it was also observed, that the uncertainty is larger for laminar flows due to smaller temperature differences and heat fluxes. For the skin friction extracted from the hot-film anemometry measurement an uncertainty of approx. $\pm 10\,\%$ is determined. Thus, the uncertainty of the TSP measurement is double the value of the hot-film measurement.

Table 4: *Measurement uncertainties of the TSP skin friction measurement.*

measurand	uncertainty
ΔT_F	$\pm$ 0.10 K
ΔU_∞	$\pm$ 0.0012 ms^{-1}
$\Delta \dot{q}_W$	$\pm$ 2 W/m^2
ΔPr	$\pm$ 0.054
Δc_p	$\pm$ 0.0002 kJ (kg K)$^{-1}$
Δx	$\pm$ 0.002 m

6. Conclusions

A Europium-based TSP, which is embedded in a PUR clear coat for aerodynamic and hydrodynamic applications, was characterized for quantitative measurements in water. The measurable emission was found to be dependent on the water content of the clear coat. After approximately two days in water a steady state of the emission is reached. A reduced transmission of UV light and visible light causes the observed behavior. Nevertheless, the temperature sensitivity of the TSP is not affected by water. These findings motivate spatial temperature measurements with TSP because temperature information with sub-millimeter resolution over large areas can be measured.

To extract skin friction information from a temperature field the Colburn analogy with an adjustment to include a delayed start of the thermal boundary layer was applied. The heat flux between model and flow was derived in areas of the undisturbed, laminar boundary, which is in good agreement with the Blasius boundary layer for the laminar water channel. This approach relies on an average temperature field which distinguishes it from the approach based on the Taylor hypothesis, where temperature fluctuations are correlated to derive the local skin friction.

In this work the average temperature field and skin friction field around two types of roughness elements were measured with TSP. The first roughness element was a single truncated cylinder, which was submerged in the laminar boundary layer, and the second type was an array of cuboids with a 45° angle to the flow direction. For the truncated cylinder the skin friction was also measured by hot film anemometry. The comparison of the results shows good agreement, which justifies the assumption for the heat flux. The second geometry is an example for a transition delay with the spanwise velocity gradient method. For a setup like this the TSP method provides large benefits, because the acquisition for a large area with high resolution is acquired in an instant. Also, it is not necessary to place a limited number of probes beforehand, which is the case for skin friction measurement techniques like Preston tubes. However, for complex setups, which deviate from the limitations of the Reynolds or Colburn analogy, the accuracy is reduced. Nevertheless, it is a suitable method for the initial evaluation of drag reduction methods. Furthermore, complex setups to capture strong velocity gradients close to the wall from the complex vortex system are not required.

The temperature and skin friction resolution are for the conditions of this measurement $(\Delta T)_{min} < 0.007\,\mathrm{K}$ and $(\Delta\tau)_{min} \leq 4.01 \times 10^{-5}\,\mathrm{N/m^2}$ ($\leq$1 %), respectively. Finally the error analysis showed that the uncertainty of the temperature measurement is dominated by the varying radiant flux of the LED and an uncertainty of the temperature measurement of $U_{\Delta T} \approx 0.3\,^\circ\mathrm{C}$ is determined. For the skin friction an uncertainty of $\pm 8.4 \times 10^{-4}\,\mathrm{N/m^2}$ (approx. $\pm$10 %) is found. The TSP method enables skin friction measurements of large areas with high spatial resolution in shorter time and on uneven surfaces. The boundary conditions of water facilities, such as the laminar water channel, are ideal for skin friction measurements with TSP due to the low temperature fluctuations.

In future a comparison of TSP results with advanced velocity measurement techniques such as particle tracking velocimetry and the possibility to perform measurements of unsteady skin friction fields needs to be investigated.

Acknowledgements The authors would like to thank T. Kleindienst (DLR-AS-EXV), C. Fuchs (DLR-AS-EXV), V. Ondrus (FH Münster), E. Mäteling (RWTH Aachen University), and M. Weberschock (Weberschock Development) for the support during the design, manufacturing and development of the TSP element. Furthermore, stimulating discussion with M. Miozzi (CNR-INSEAN) gave vital impulses to the data evaluation.

References

G. Ahlers, S. Grossmann, and D. Lohse. Heat transfer and large scale dynamics in turbulent Rayleigh-Bénard convection. *REVIEWS OF MODERN PHYSICS*, 81:503–537, 2019. doi: 10.1103/RevModPhys.81.503.

A.-M. Bouchardy, G. Durand, and G. Gauffre. Processing of infrared thermal images for aerodynamic research. In *Applications of Digital Image Processing V*, pages 304–309, 1983. doi: 10.1117/12.935316.

H. Buiteveld, J.H.M. Hakvoort, and M. Donze. Optical properties of pure water. In *Ovean Optics XII*, pages 105–122, 1994. doi: 10.1117/12.190060.

L.N. Cattafesta, T. Liu, and J.P. Sullivan. Uncertainty estimates for temperature-sensitive paint measurements with charge-coupled device cameras. *AIAA Journal*, 36 (11):2102–2108, 1998.

T. Cebici and P. Bradshaw. *Physical and Computational Aspects of Convective Heat Transfer*. Springer, 1984.

A.P. Colburn. A method of correlating forced convection heat transfer data and a comparison with fluid friction. In *Trans. Am. Inst. Chem. Engrs*, volume 29, pages 174–210, 1933.

Y. Egami, C. Klein, U. Henne, M. Bruse, V. Ondrus, and U. Beifuß. Development of a highly sensitive temperature-sensitive paint for measurements under ambient (0-60) conditions. In *47th AIAA Aerospace Sciences Meeting Including The New Horizons Forum and Aerospace Exposition, 5-8 January 2009, Orlando, Florida*. AIAA 2009-1075, 2009.

U. Fey and Y. Egami. *Springer Handbook of Experimental Fluid Mechanics*, chapter Transition-Detection by Temperature-Sensitive Paint. Springer-Verlag, Berlin, Heidelberg, 2007.

S.D. Fonov, L.P. Goss, G.E. Jones, J.W. Crafton, and V.S. Fonov. New method for surface pressure measurements. In *43rd AIAA Aerospace Sciences Meeting and Exhibit, 10 - 13 January 2005, Reno, USA*. AIAA 2005-1029, 2005. doi: DOI:10.2514/6.2005-1029.

J. H. M. Fransson, L. Brandt, A. Talamelli, and C. Cossu. Experimental study of the stabilization of Tollmien-Schlichting waves by finite amplitude streaks. *Phys. Fluids*, 17(054110):10, 2005. doi: doi.org/10.1063/1.1897377.

L. Gaudet and T.G. Gell. Use of liquid crystals for qualitative and quantitative 2-D studies of transition and skin friction. In *International Congress on Instrumentation in Aerospace Simulation Facilities*, pages 66–81, 1989. doi: 10.1109/ICIASF.1989.77660.

N. Gregory and W.S. Walker. The effect on transition of isolated surface excrescences in the boundary layer. Technical report, ARC Rep., R. & M. No. 2779, 1956.

G. Groskopf, M. J. Kloker, and K. A. Stephani. Temperature / rarefaction effects in hypersonic boundary-layer flow with an oblique roughness element. In *41st AIAA Fluid Dynamics Conference and Exhibit, 27-30 Juni 2011, Honolulu, USA*. AIAA 2011-3251, 2011.

F. Haselbach, M. Baumann, D. Sturzebecher, and W. Nitsche. Visualization of flow instabilities and forced transition by means of heated liquid crystal foils. In *Proceedings of the Seventh International Symposium on Flow Visualization*, 1995.

Nicholas M. Husen, Tianshu Liu, and John Sullivan. *The Luminescent Oil-Film Flow-Tagging (LOFFT) Skin-Friction Meter Applied to FAITH Hill*. 2017. doi: 10.2514/6.2017-0481. URL `https://arc.aiaa.org/doi/abs/10.2514/6.2017-0481`.

Y. Iijima, Y. Egami, A. Nishizawa, K. Asai, U. Fey, and R.H. Engler. Optimization of temperature-sensitive paint formulation for large-scale cryogenic wind tunnels. In *20th International Congress on Instrumentation in Aerospace Simulation Facilities (ICIASF), Göttingen, Deutschland, 25–29 August 2003*, pages 70–76, 2003.

C. Klein, R. Engler, U. Henne, and W. Sachs. Application of pressuresensitive paint for determination of the pressure field and calculation of the forces and moments of models in a wind tunnel. *Experiments in Fluids*, 39:475–483, 2005. doi: 10.1007/s00348-005-1010-8.

E.J. Klein. Application of liquid crystals to boundary-layer flow visualization. In *AIAA 3rd Aerodynamic Testing Conference, San Francisco, USA*. AIAA 68-376, 1968. doi: 10.2514/6.1968-376.

E.J. Klein and A.P. Margozzi. Apparatus for the calibration of shear sensitive liquid crystals. *Review of Scientific Instruments*, 41:238–239, 1970.

M. Kruse and S. Wagner. Visualization and laser Doppler measurements of the development of Lambda vortices in laminar-turbulent transition. *Meas. Sci. Technol.*, 9(4): 659–669, 1998.

Y. Le Sant, M. Marchand, P. Millan, and J. Fontaine. An overview of infrared thermography techniques used in large wind tunnels. *Aerospace Science and Technology*, 6: 355–366, 2002. doi: 10.1016/S1270-9638(02)01172-0.

J. Lemarechal, C. Klein, U. Henne, D.K. Puckert, and U. Rist. Transition delay by oblique roughness elements in a Blasius boundary-layer flow. In *AIAA SciTech Forum 2018 AIAA Aerospace Sciences Meeting*. AIAA 2018-1057, 2018. doi: 10.2514/6.2018-1057.

J. Lemarechal, C. Klein, U. Henne, D.K. Puckert, and U. Rist. Detection of lambda- and omega-vortices with the temperature-sensitive paint method in the late stage of controlled laminar-turbulent transition. *Experiments in Fluids*, 60:91:1–14, 2019. doi: 10.1007/s00348-019-2734-1.

J. Lemarechal, E. Mäteling, C. Klein, D. Puckert, and U. Rist. Visualization of near-wall structures of an isolated cylindrical roughness element in a laminar boundary layer without pressure gradient. In A. Dillmann, G. Heller,

E. Krämer, C. Wagner, C. Tropea, and S. Jakirlić, editors, *New Results in Numerical and Experimental Fluid Mechanics XII*, pages 674–683. Springer, Cham, 2020. doi: 10.1007/978-3-030-25253-3_64.

H.-T. Lin. The analogy between fluid friction and heat transfer of laminar forced convection on a flat plate. *Wärme- und Stoffübertragung*, 29:181–184, 1994.

T. Liu and J. P. Sullivan. *Pressure And Temperature Sensitive Paints*. Springer-Verlag Berlin Heidelberg, 2005.

T. Liu and S. Woodiga. Feasibility of global skin friction diagnostics using temperature sensitive paint. *Meas. Sci. Technol.*, 115402(22):11, 2011. doi: 10.1088/0957-0233/22/11/115402.

T. Liu, B. Campbell, and J. Sullivan. Accuracy of temperature-sensitive fluorescent paint for heat transfer measurements. In *30th AIAA Thermophysics Conference, 19-22 Juni 1995, SanDiego, CA, USA*. AIAA 95-2042, 1995.

Luminus Devices, Inc. *CBT-120-UV Product Datasheet*, 2016.

M. Miozzi, A. Capone, F. Di Felice, C. Klein, and T. Liu. Global and local skin friction diagnostics from tsp surface patters on an underwater cylinder in crossflow. *PHYSICS OF FLUIDS*, 28(124101), 2016.

M. Miozzi, A. Capone, M. Costantini, L. Fratto, C. Klein, and F. Di Felice. Skin friction and coherent structures within a laminar separation bubble. *Experiments in Fluids*, 60:13, 2019a. doi: 10.1007/s00348-018-2651-8.

M. Miozzi, C. Klein, F. Di Felice, and M. Costantini. Incipient stall characterization from skin friction maps. In *54th 3AF International Conference on Applied Aerodynamics, 25–27 March 2019, Paris, France*, 2019b.

K. Nakakita, T. Osafune, and K. Asai. Global heat transfer measurement in a hypersonic shock tunnel using temperature sensitive paint. In *41st AIAA Aerospace Sciences Meeting, 6–9. January, 2003, Reno, Nevada, USA*. AIAA 2003-0743, 2003.

V. Ondrus, R. J. Meier, C. Klein, U. Henne, M. Schäferling, and U. Beifuß. Europium 1,3-di(thienyl)propane-1,3-diones with outstanding properties for temperature sensing. *Sensors and Actuators, A: Physical*, 233:434–441, 2015. doi: 10.1016/j.sna.2015.07.023.

PCO AG. *pco.camera Benutzerhandbuch*. Kehlheim, Deutschland, 12 2004.

D.J. Peake, A.J. Bowker, S.J. Lockyear, and F.A. Ellis. Non-obtrusive detection of transition region using an infrared camera. *AGARD-CP-224*, 1977.

D.K. Puckert, M. Dieterle, and U. Rist. Reduction of freestream turbulence at low velocities. *Exp. Fluids*, 58 (45), 2018. doi: DOI10.1007/s00348-017-2333-y.

A. Quast. Detection of transition by infrared image technique. In *12th International Congress on Instrumentation in Aerospace Simulation Facilities (ICIASF87), 22-25 Juni 1987, Williamsburg, USA*, pages 125–134, 1987.

D.C. Reda and J.J. Muratore. Measurement of surface shear stress vectors using liquid crystal coatings. *AIAA J.*, 32 (8):1576–1582, 1994.

O. Reynolds. On the extent and action of the heating surface for steam boilers. In *Proc. Manchester Lit. Phil. Soc.*, volume 14, pages 7–12, 1874.

I. Rudolph. *Infrared Thermography as a Tool for Wall Shear Stress Measurements*. PhD thesis, TU Berlin, 2011.

R. Sedney. A survey of the effects of small proturbances on boundary-layer flows. *AIAA Journal*, 11(6):782–792, 1973. doi: 10.2514/3.50520.

M. Strunz. *Ein Laminarwasserkanal zur Untersuchung von Stabilitätsproblemen in der Strömungsgrenzschicht*. PhD thesis, University of Stuttgart, 1987.

A Subasi, D. Puckert, H. Gunes, and U. Rist. Calibration of constant temperature anemometry with hot-film probes for low speed laminar water channel flows. In *13th International Symposium on Fluid Control, Measurement and Visualization FLUCOME2015, 15-18 November, Doha, Qatar*, 2015.

H. Thomann and B. Frisk. Measurement of heat transfer with an infrared camera. *Int. J. Heat Mass Transf.*, 11:819–826, 1968. doi: 10.1016/0017-9310(68)90126-9.

M.J. Walsh. *Viscous Drag Reduction in Boundary Layers*, chapter Riblets, pages 203–261. AIAA Inc., 1990. doi: 10.2514/5.9781600865978.0203.0261.

P. Wassermann and M. Kloker. Mechanisms and passive control of crossflow-vortexinduced transition in a three-dimensional boundary layer. *J. Fluid Mech.*, 456:49–84, 2002. doi: 10.1017/S0022112001007418.

T. Wiegand, H. Bestek, S. Wagner, and H. Fasel. Experiments on a wave train emanating from a point source in a laminar boundary layer. In *26th AIAA Fluid Dynamics Conference, 19-22 Juni 1995, San Diego, USA*. AIAA-95-2255, 1995.

S. Zhong, C. Kittichaikan, H.P. Hodson, and P.T. Ireland. Visualization of turbulent spots and unsteady wake-induced boundary-layer transition with thermochromic liquid crystals. *Optics & Laser Technology*, 31:33–39, 1999. doi: 10.1016/S0030-3992(99)00022-5.